



HAL
open science

Solvent Key Parameters for the Wet Chemical Synthesis of the Li₃PS₄ Solid Electrolyte

Romain Poirier, David Pasquier, Arnold Lambert, Manuel Corral Valero,
Denis Uzio, Cyril Garnero

► **To cite this version:**

Romain Poirier, David Pasquier, Arnold Lambert, Manuel Corral Valero, Denis Uzio, et al.. Solvent Key Parameters for the Wet Chemical Synthesis of the Li₃PS₄ Solid Electrolyte. *Journal of Physical Chemistry C*, 2024, 128 (28), pp.11477-11486. 10.1021/acs.jpcc.4c01598 . hal-04696178

HAL Id: hal-04696178

<https://ifp.hal.science/hal-04696178v1>

Submitted on 12 Sep 2024

HAL is a multi-disciplinary open access archive for the deposit and dissemination of scientific research documents, whether they are published or not. The documents may come from teaching and research institutions in France or abroad, or from public or private research centers.

L'archive ouverte pluridisciplinaire **HAL**, est destinée au dépôt et à la diffusion de documents scientifiques de niveau recherche, publiés ou non, émanant des établissements d'enseignement et de recherche français ou étrangers, des laboratoires publics ou privés.

Solvent key parameters for the wet chemical synthesis of Li_3PS_4 solid electrolyte.

*Romain POIRIER^a, David PASQUIER^a, Arnold LAMBERT^a, Manuel CORRAL VALERO^a,
Denis UZIO^a and Cyril GARNERO^{a*}*

^aIFP Energies Nouvelles, Rond-point de l'échangeur de Solaize, BP3, 69360 Solaize, France

*Corresponding Author Email : cyril.garnero@ifpen.fr

Abstract

Solid sulfide electrolytes hold great promise for making all solid-state batteries a reality. Therefore, their wet chemical synthesis has become increasingly important in recent years due to various benefits such as scalability and versatility. Li_3PS_4 electrolyte has a relatively high ionic conductivity ($\approx 10^{-4} \text{ S.cm}^{-1}$ at 25°C) and can be synthesized in various organic solvents by reacting Li_2S and P_2S_5 . It is well known that the choice of the solvent is critical for the synthesis. Herein, we investigated several new organic polar solvents such as sulfur-based solvents (propanethiol, thiolane, thiophene), amines and carbonyls (esters, carbonates, ketones) for the synthesis of Li_3PS_4 . The relationship between the ability to perform the reaction, the ionic conductivity and the solvents' characteristics revealed that the electronic density of the polar function plays a key role. The results of this study can be used as a guideline to select new synthesis solvents. We also identify a particular solvent, isobutyl isobutyrate (IBIB), which allows the decomposition of the corresponding Li_3PS_4 solvato-

complex below the boiling point of the solvent with one of the highest ionic conductivities for the wet chemical method ($2.1 \times 10^{-4} \text{ S.cm}^{-1}$ at room temperature).

Keywords: Wet chemical synthesis, solid electrolyte, Li_3PS_4 , solvent

Introduction

For many years now, research has been carried out to achieve new generations of more efficient and safer batteries. Indeed, current Li-ion batteries use organic liquid electrolytes that are flammable, harmful and can lead to cell explosion (1). Therefore, several research groups are developing all-solid state batteries with expected higher energy density, reliability and improved safety thanks to the use of solid electrolytes based on polymers, inorganic phases or hybrid electrolytes (2). Among inorganic electrolytes, sulfide based materials present some advantages such as a high ionic conductivity ($> 10^{-4}$ S.cm⁻¹) and cold densification due to a high ductility (1). This category includes the Li₂S-P₂S₅ system (LPS) with Li₃PS₄ (3) and Li₇P₃S₁₁ (4), as well as argyrodites Li₆PS₅X (LPSX, X = Cl, Br, I) (5), and Li_{4-x}Ge_{1-x}P_xS_{4x} (LGPS) (6). These materials are usually prepared by a melting-quench method or mechanochemical synthesis, which allows to obtain the phases with a good purity and high ionic conductivity. However, such syntheses are time-consuming and energy intensive, limiting their scalability (1). To address this issue, several research groups attempt to synthesize these phases by the liquid route: LPS (7–10); LPSX (11–14); LGPS (15, 16).

In the case of Li₃PS₄, the first liquid phase synthesis was performed in tetrahydrofuran (THF) by Liu *et al.* (9). They stirred a suspension of Li₂S and P₂S₅ (molar ratio = 3 : 1) in THF during 24 h at room temperature and obtained the intermediary solvato-complex compound Li₃PS₄·2THF. After heat treatment, the pure β-Li₃PS₄ phase was obtained with an ionic conductivity of 1.6×10^{-4} S.cm⁻¹ at 25°C. Calpa *et al.* (17, 18) reported the use of acetonitrile (ACN) to synthesize β-Li₃PS₄ and suggested a mechanism for its formation. THF (19, 20) and ACN (21, 22), have become usual solvents for LPS wet synthesis, along with 1,2 dimethoxyethane (DME) (18) and ethyl acetate (EA) (23, 24). However, the precursors (Li₂S and P₂S₅) are poorly or not soluble in

such aprotic polar solvents. As a consequence slow reaction kinetics are observed because the reaction takes place only on the surface of Li_2S particles (7). To overcome this, other solvents have been investigated, including amines which can fully dissolve the precursors thanks to their protic nature (25, 26). Ito *et al.* (25) synthesized Li_3PS_4 by mixing Li_2S and P_2S_5 in ethylenediamine (EDA) for 3 h at room temperature. After solvent evaporation at 200°C , a heat treatment was performed at 260°C to obtain $\beta\text{-Li}_3\text{PS}_4$ ($\sigma = 5.0 \times 10^{-5} \text{ S.cm}^{-1}$). However, the products obtained using protic solvents exhibit low ionic conductivity, which has been attributed to impurities that crystallize along with the $\beta\text{-Li}_3\text{PS}_4$ phase (26).

Despite all these studies, the effect of the solvent on the solvato-complex formation, on its decomposition and on the resulting material's ionic conductivity remains unclear, as does the reason why THF is the optimal solvent for the wet chemical synthesis of Li_3PS_4 . Several attempts have been made in the literature, to explain the ability to form Li_3PS_4 in suspension by studying solvents properties. For example, Matsuda *et al.* studied the impact of solvents' electronic density on the Li_3PS_4 formation by using solvents with different carbonyl moieties (carbonate, acetate and ketone) (23). Takahashi *et al.* (27) examined the effect of the solvents' boiling point on the resulting materials' ionic conductivity. They showed a relationship between the crystallinity of the Li_3PS_4 phase and the boiling point of the solvent used for the synthesis. They concluded that low boiling point solvents mainly lead to an amorphous structure after decomposition of the solvato-complex. In wet chemical synthesis, Li_3PS_4 materials show better ionic conductivity for poor crystallized phases (1, 27). Yamamoto *et al.* compared several acetates (EA, butyl acetate (BA) or propyl acetate (PA)) to establish a correlation between measured ionic conductivities, Hansen parameters (polarity, hydrogen bonding) and solvents' boiling point. They observed an impact of the coordination of the PS_4^{3-} tetrahedra by the solvent

and found that a low coordination number is beneficial to the ionic conductivity (BA, $\sigma = 5 \times 10^{-4}$ S.cm⁻¹). They attributed the low coordination number of PS₄³⁻ with BA to its poor affinity with Li₃PS₄. This low coordination induces decomposition of the solvato-complex to β -Li₃PS₄ at a temperature below the solvent's boiling point leading to a poor crystallinity of Li₃PS₄ and the highest ionic conductivity for wet chemical synthesis method. The Li₃PS₄·BA solvato-complex is the unique case of early decomposition in the literature. Similarly, Gamo *et al.* (21) benchmarked the synthesis of Li₇P₃S₁₁ in various solvents to understand the impact of different parameters such as boiling point, steric hindrance or dielectric constant. In fact, many papers indicate some parameters (28) such as the boiling point (8, 27, 21), dielectric constant (21) or Hansen's parameter (8) as key parameters for LPS synthesis, but no link has been established in the literature between these parameters and comparisons were only performed on a limited number of chemical families of solvents (esters, amines).

In this work, we studied various new solvents with different properties to synthesize Li₃PS₄ and assessed the resulting ionic conductivities. We aimed at establishing a connection between the different properties (polarity, dielectric constant, boiling point, functional group) of the tested solvents as well as previously reported solvents. These properties determine the ability to form a solvato-complex during the wet synthesis and impact its further decomposition, as well as the ionic conductivity measured on the final material.

Therefore, different functional groups derived from previously reported syntheses were tested such as esters, ketones, amines and alkyl carbonates. We also introduced sulfur based functional groups such as thiols, thioethers and one sulfone which have not yet been tested in the wet chemical synthesis of Li₃PS₄. Through our research, we succeeded in identifying a new solvent, isobutyl isobutyrate, which allows the crystallization of the β -Li₃PS₄ phase at a lower

temperature than its boiling point and leads to one of the highest measured ionic conductivities for this kind of synthesis method.

Methods

All solvents: n-butylamine (Alfa Aesar, +99%), 1-3 diaminopropane (Aldrich, 99%), 1-propanethiol (Thermo scientific, 98%), tetrahydrothiophene (Aldrich, 99%), thiophene (Aldrich, +99%), dimethyl disulfide (Aldrich, 99%), sulfolane (Thermo scientific, 99%), propylene carbonate (Aldrich, 99%), dimethyl carbonate (Aldrich, 99%), isobutylisobutyrate (Thermo scientific, 98%), methylisobutylketone (Supelco, 99%) were dried with activated 3Å molecular sieve before use. Sulfide precursors Li_2S (Aldrich, 99.98%) and P_2S_5 (Aldrich, 99%) were used as received. All processes were performed under argon atmosphere (glove box; $\text{H}_2\text{O} \leq 0.1$ ppm; $\text{O}_2 \leq 0.1$ ppm) to avoid hydrolysis of the sulfide materials and their precursors.

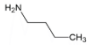

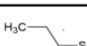
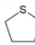
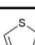
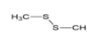
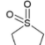
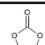
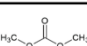
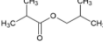
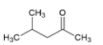
Solvents	Molecular structure	T_{ebu} (°C)	δ_p (MPa ^{-1/2})	ϵ	$\mu_D \times 10^{30}$ (c.m)
n-butylamine		78	4,75	35,09	4,64
1-3 Diaminopropane		139	-	12,5	6,14
1-Propanethiol (PSH)		68	6,3	5,95	5,14
Tetrahydrothiophene (THT)		119	6,7	8,61	6,34
Thiophene		84	2,4	2,74	1,8
Dimethyle Disulfide (DMS)		110	7,8	9,6	6,62
Sulfolane		285	18,2	43,26	15,6
Propylene carbonate (PC)		242	18	66,14	16,6
Dimethyl carbonate (DMC)		90	3,9	3,08	3
Isobutyl isobutyrate (IBIB)		145	2,9	4,76	6,5
Methyl isobutylketone (MIBK)		116	6,1	15,6	8,97

Table 1 : List of solvents and their parameters

Syntheses

Li₂S and P₂S₅ were mixed in the solvents listed in Table 1 for 72 h at 50°C. In most cases, a dispersion was obtained and was centrifugated at 10000 rpm during 15 min. Then the powder was vacuum-dried at the solvent's boiling temperature. With amines, a solution was obtained, which was evaporated under vacuum at the solvent's boiling temperature to obtain the solvato-complex Li₃PS₄·solvent. The dried powder is then characterized. The drying temperature is set close to the boiling point of the synthesis solvent for the heavy solvents or below for the volatile ones: n-butylamine (50°C); 1-3 diaminopropane (140°C), 1-propanethiol (25°C), tetrahydrothiophene (25°C), thiophene (25°C), dimethyl disulfide (50°C), sulfolane (260°C), propylene carbonate (120°C), dimethyl carbonate (25°C), isobutyl isobutyrate (120°C), methyl isobutyl ketone (120°C).

Decomposition of solvato-complexes

The decomposition temperature of each solvato-complex has been determined by thermogravimetric analysis. Selected solvato-complexes were then decomposed under argon flow for 4 h at their decomposition temperature to obtain the Li₃PS₄ phase, which was further characterized.

Analysis

X-ray diffraction measurements were performed with a Bruker D4 diffractometer (40 kV, 40 mA) and a copper anode ($K\alpha_1 = 1,54060 \text{ \AA}$; $K\alpha_2 = 1,54439 \text{ \AA}$) at room temperature. The samples were prepared with a transmission device and Kapton[®] sheets sealed with vacuum grease. This setup generates a characteristic amorphous signal between 15° and 30° (Supporting

info 1 (S1)). Li_2S and $\beta\text{-Li}_3\text{PS}_4$ structures were indexed with the PDF cards n°00-026-1188 and n°04-010-1784 respectively.

Raman spectroscopy was performed with a Renishaw spectrometer (confocal lens and 532 nm laser). Some compounds subject to fluorescence were analyzed with a 1064 nm laser. The laser power used is 0,75 mW and 43 mW for the 532 nm laser and 1064 nm laser respectively. Hermetic glass cells were used to make the measurements under argon at room temperature.

Thermogravimetric analyses were carried out using a Mettler TGA-DSC-1 instrument in an alumina crucible under nitrogen flow at a rate of 25 mL/min up to 500°C with a heating ramp of 5°C/min. The samples were weighted in the glove box and transported in an air-tight container. The crucible was then swiftly introduced with N_2 flowing through the chamber. The air exposition of the sample was less than 10 sec.

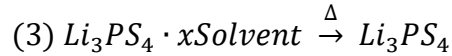
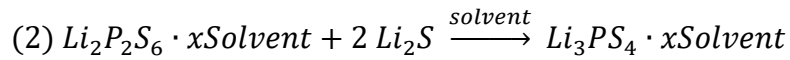
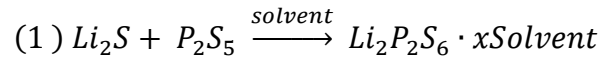
Ionic conductivity measurements were carried out by electrochemical impedance spectroscopy (EIS) using a BioLogic MTZ-35 impedance analyzer connected to a Sphere Energy 8 mm diameter cell. The powder was directly densified within the cell at 390 MPa between two blocking electrodes (stainless steel) for 5 min at room temperature. EIS measurements were performed at this pressure at 25°C with the following acquisition parameters: DC potential 0 V, $\Delta V = \pm 60$ mV, frequency range 1 MHz - 1Hz. The voltage perturbation was chosen to enhance the signal to noise ratio.

Atomic charges were obtained from a Mulliken Population Analysis based on structures optimized within the framework of Density Functional Theory (DFT) as implemented in the DMol3 package (29, 30). We used the hybrid exchange-correlation functional from Becke-Lee-Yang-Parr (B3LYP) (31, 32) and a double-numerical basis including a polarization d-function. The convergence criteria for electronic structure calculations were 2.0×10^{-5} Ha for the energy

and 1.0×10^{-5} a.u. for the electron density. Geometry optimizations were considered to be converged when the energy between cycles was below the 2.0×10^{-5} Ha threshold and either the maximum force or the maximum displacement below 4.0×10^{-3} Ha/Å and 5.0×10^{-3} Å, respectively.

Results & discussion

Several studies have highlighted the reaction path for the formation of the Li_3PS_4 phase (18, 19, 9). Basically, the reaction of Li_2S and P_2S_5 takes place with a 3:1 molar ratio within polar (mostly aprotic) solvents. It can be described by the following three-step mechanism:



The first step (eq 1) entails the formation of the intermediate solvato-complex $\text{Li}_2\text{P}_2\text{S}_6 \cdot x\text{Solvent}$ through the equimolar reaction of Li_2S with P_2S_5 (19). This intermediate is soluble and its formation isn't the limiting step of the reaction. Therefore, this reaction is usually complete and thus the P_2S_5 is totally consumed when the solvent allows the reaction. The second step (eq 2) is the reaction of the two remaining equivalents of Li_2S with the intermediate solvato-complex (limiting step) to form the final solvato-complex $\text{Li}_3\text{PS}_4 \cdot x\text{Solvent}$. Due to the poor solubility of the Li_2S precursor, this reaction takes place on the surface of Li_2S and so the size of initial Li_2S particles determine the size of the final compound (33). Therefore, the presence of unreacted Li_2S after the reaction is usually a sign of slow reaction kinetics and unfinished reaction. The last step (eq 3) is the thermal decomposition of the solvato-complex to obtain the Li_3PS_4 phase.

Depending on the annealing conditions, the crystalline β phase or an amorphous phase can be obtained (9, 8).

Based on this mechanism, we first assessed the formation of the $\text{Li}_3\text{PS}_4 \cdot x\text{Solvent}$ solvato-complexes in the different solvents. The tested solvents and their properties are listed in table 1. All syntheses were performed at 50°C for 72 h to ensure the reaction completion. For comparison purposes, the synthesis was carried out in tetrahydrofuran (THF) and acetonitrile (ACN), using the reported conditions (9, 18). The Raman and XRD characterizations presented in Figure 1G and 1H confirm the formation of $\text{Li}_3\text{PS}_4 \cdot 2\text{THF}$ and $\text{Li}_3\text{PS}_4 \cdot 2\text{ACN}$ in agreement with the references (9, 18, 20).

Figure 1A and 1B present the Raman spectra and XRD diffractograms of the powders obtained with two amino solvents. In the case of n-butylamine, the P_2S_5 signature is not present, showing that the formation of the solvato-complex $\text{Li}_2\text{P}_2\text{S}_6 \cdot x\text{solvent}$ in step 1 has indeed taken place. The formation of the PS_4^{3-} units is confirmed at 419 cm^{-1} by Raman spectroscopy (Figure 1A) (20). The XRD pattern shows the presence of an unknown crystal structure, that could not be identified in the ICDD database (Figure 1B), as well as that of Li_2S . It is noteworthy that only a few crystal structures of solvato-complexes such as $\text{Li}_3\text{PS}_4 \cdot \text{ACN}$ (Figure 1H) (17), $\text{Li}_3\text{PS}_4 \cdot \text{DME}$ (18), $\text{Li}_3\text{PS}_4 \cdot \text{EDA}$ (26) and $\text{Li}_3\text{PS}_4 \cdot 2\text{NMF}$ (34) have been fully resolved. Also, for other solvents, it is common for XRD patterns of powders to reveal unknown crystalline structures which are converted to $\beta\text{-Li}_3\text{PS}_4$ or amorphous Li_3PS_4 upon annealing (8, 35, 36). Therefore, the formation of a new crystallized solvato-complex is mainly deduced from the dissimilarity to other known XRD patterns and the presence of PS_4^{3-} units in Raman spectra. The XRD peak at $6.5^\circ 2\theta$ could indicate the presence of a lamellar solvato-complex similar to those induced by THF (Figure

^1H (9, 20) and acetates (7). The formation of the $\text{Li}_3\text{PS}_4 \cdot x\text{Solvent}$ solvato-complex is a two-step process.

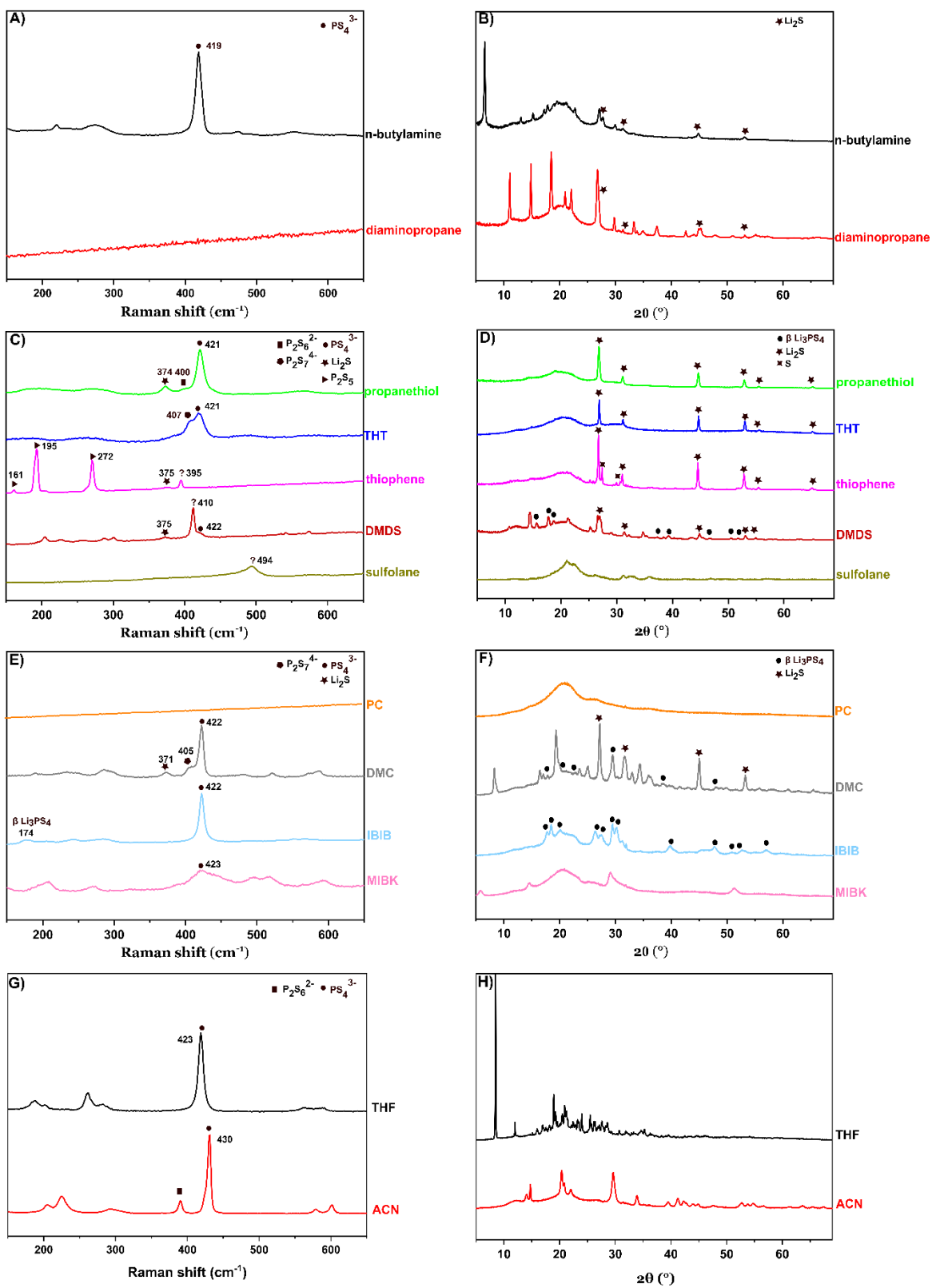


Figure 1 : Raman spectrum (A, C, E) and XRD data (B, D, F) of $\text{Li}_3\text{PS}_4 \cdot x\text{Solvent}$ after syntheses compared to the established synthesis' solvents: THF and ACN (G, H).

The powder obtained in diaminopropane is a mixture of an unknown crystalline phase and traces of Li_2S . This phase is probably a solvato-complex structure between Li_3PS_4 and diaminopropane. Given the strong fluorescence background in Figure 1A, no conclusion can be drawn from this Raman spectrometer equipped with a 532 nm laser. An additional RAMAN analysis using a 1064 nm laser (S2) has been performed and confirmed Li_3PS_4 formation with a peak at 421 cm^{-1} . XRD analysis (Figure 1B) of the phases synthesized in the amino solvents shows the characteristic signature of the Li_2S precursor. The amino solvents form a relatively stable complex with P_2S_5 (green solution) (25, 10) which may explain the lower reactivity of this precursor and the presence of residual Li_2S .

Figure 1C and 1D present Raman spectra and XRD patterns, respectively, of powders obtained with sulfur-containing solvents. For the synthesis in propanethiol (PSH), the Raman spectrum exhibits the characteristic peak of PS_4^{3-} at 421 cm^{-1} with two other peaks at 374 cm^{-1} and 400 cm^{-1} which can be attributed to Li_2S and $\text{P}_2\text{S}_6^{2-}$, respectively (1). Moreover, the two wide peaks in the network vibration zone ($150 \text{ cm}^{-1} - 300 \text{ cm}^{-1}$) could suggest an amorphous structure of Li_3PS_4 (20). XRD analysis only shows the presence of Li_2S (Figure 1D). Thus, a vacuum drying step at the PSH boiling point (68°C) induces an amorphous phase by decomposing the solvato-complex. Since Li_2S is less responsive in Raman spectroscopy than in XRD (7), we can deduce that a significant amount of Li_2S did not react due to slow reaction kinetics.

In the case of tetrahydrothiophene (THT), despite its similarity to THF, only the presence of Li_2S was observed by XRD (Figure 1D). The PS_4^{3-} unit was however detected in Raman spectroscopy

(421 cm^{-1}) along with $\text{P}_2\text{S}_7^{4-}$ units (407 cm^{-1}) (1). This can be explained by a decomposition of the solvato-complex at the drying temperature, by analogy with the previous PSH case. Here, the formation of $\text{P}_2\text{S}_7^{4-}$ may be due to a reaction occurring during drying between $\text{Li}_3\text{PS}_4\cdot\text{THT}$ and residual $\text{Li}_2\text{P}_2\text{S}_6\cdot\text{THT}$ that may not have been eliminated by centrifugation (19). The difference in reactivity between THF and THT as solvents may be due to the higher electronegativity of oxygen compared to sulfur, imparting higher interaction of Li_3PS_4 with THF than with THT.

In thiophene, it appears that the reaction between Li_2S and P_2S_5 does not take place, since only the reactants are detected by both XRD and Raman spectroscopy after 72 h of reaction (Li_2S and P_2S_5 at 375 cm^{-1} and between 150 cm^{-1} and 275 cm^{-1} (37) respectively). Actually, the presence of P_2S_5 means that no reaction occurred because the formation of the first solvato-complex (step 1) $\text{Li}_2\text{P}_2\text{S}_6\cdot x \text{Solvent}$ is generally fast (19). The lack of reaction between Li_2S and P_2S_5 was also observed in furan, which will be further reported in a forthcoming publication. The fact that thiophene and furan are the only solvents tested in which no reaction occurs may indicate that compounds with an aromatic ring are not suitable candidates for Li_2S - P_2S_5 reaction.

In dimethyl disulfide (DMDS), XRD analysis of the solid obtained indicates that the crystalline β phase has indeed been formed as well as an unknown structure. Traces of unreacted Li_2S are also detected (Figure 1D). The Raman spectrum confirms the presence of Li_2S and PS_4^{3-} (422 cm^{-1}). However, the peak at 410 cm^{-1} (Figure 1C) is rather low to be attributed to PS_4^{3-} units and too high to match $\text{P}_2\text{S}_7^{4-}$ units. This environment is probably originated from the unknown crystalline phase detected by XRD.

With sulfolane, the results are difficult to interpret because the X-ray pattern (Figure 1D) is mostly amorphous with no characteristic peaks. The Raman spectrum (Figure 1C) shows a single

peak at 494 cm^{-1} which is not related to the PS_4^{3-} unit. We can only conclude that this solvent does not seem relevant for the wet chemical synthesis of Li_3PS_4 .

Figure 1E and 1F show the results obtained for solvents with carbonyl functions. Let's consider alkyl carbonates. In DMC, a mixture of solvato-complex and β -phase is obtained, and traces of Li_2S are detected. This mixture can be explained by a degradation of the solvato-complex by the solvent during the 72 h of reaction. Indeed, Shimamoto *et al.* (38) indicate that Li_3PS_4 and alkyl carbonates tend to react together to form Li_2S , a reaction that is accompanied by solvent decomposition (CO_2 formation). Production of CO_2 probably occurred under our reaction conditions, as evidenced by the ejection of a cap due to pressure buildup after around 4 h of stirring. This implies a degradation involving the DMC solvent and the solvato-complex.

In PC, the same phenomenon takes place and the reaction leads to an amorphous phase with no trace of Li_2S (Figure 1E). Strong fluorescence during Raman acquisition prevents any confirmation of Li_3PS_4 formation.

Synthesis in methyl isobutyl ketone (MIBK) results in the formation of a poorly crystalline structure which may be assigned to a solvato-complex and/or an amorphous phase (Figure 1F). The Raman spectrum presents a poorly defined environment of " PS_4^{3-} " units (Figure 1E).

Finally, isobutyl isobutyrate (IBIB) allows the formation of the β -phase without any impurities as shown in the XRD diffractogram (Figure 1F). That is confirmed by Raman spectroscopy with a unique PS_4^{3-} environment (422 cm^{-1}), network vibrations ($200 - 300\text{ cm}^{-1}$) and a peak at 174 cm^{-1} corresponding to the crystalline phase $\beta\text{-Li}_3\text{PS}_4$ (20). The drying temperature (120°C) seems to be sufficient to decompose the solvato-complex. Therefore, the synthesis was reproduced with a drying step at room temperature instead of 120°C . XRD and Raman analyses (S3) confirm the

formation of a $\text{Li}_3\text{PS}_4 \cdot x\text{IBIB}$ solvato-complex structure without any impurities. The XRD pattern shows an amorphous phase with no traces of Li_2S while the Raman spectrum attests to the formation of the PS_4 units with a peak at 422 cm^{-1} . Thermogravimetric analysis (Figure S3) shows a first mass loss at 100°C before the boiling point of IBIB (120°C). This means that the solvato-complex $\text{Li}_3\text{PS}_4 \cdot x\text{IBIB}$ decomposes below the boiling point of the solvent. This behavior is similar to the work of Yamamoto *et al.* with butyl acetate where the bulkiness of the solvent leads to a poorly crystallized solvato-complex which decomposes below the boiling point of the solvent (8). The $\text{Li}_3\text{PS}_4 \cdot x\text{IBIB}$ solvato-complex was decomposed at 100°C for 2 h (characterization in S3).

As described in equation 3, the thermal decomposition of the Li_3PS_4 solvato-complexes leads to the formation of β - and/or amorphous Li_3PS_4 structure. From the previous XRD and Raman analyses, PSH, THT, DMDS and IBIB solvents produced either crystalline or amorphous Li_3PS_4 without additional heat treatment, while thiophene didn't allow the reaction between Li_2S and P_2S_5 . Therefore, only compounds presenting a solvato-complex structure were annealed to be decomposed into the β phase.

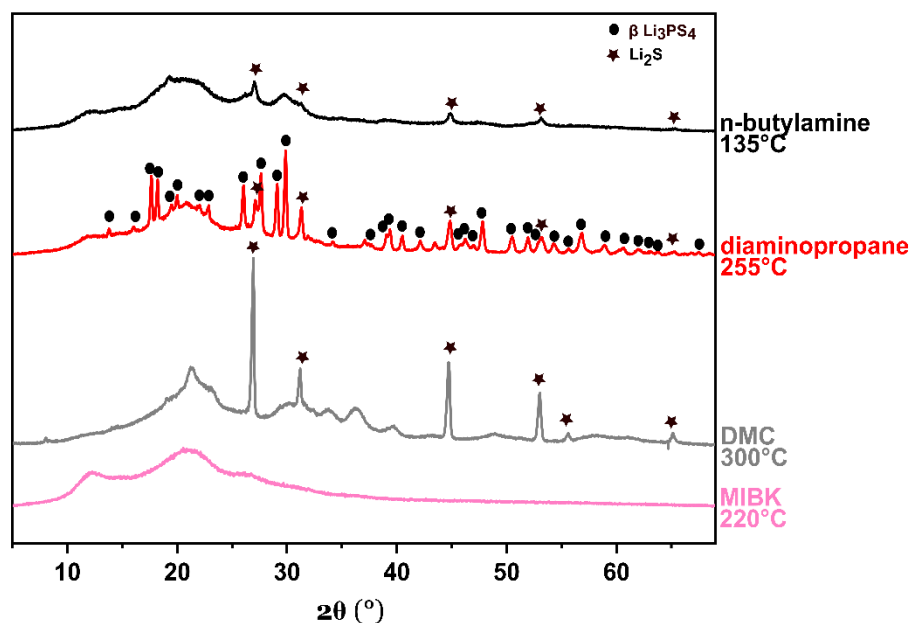


Figure 2 : XRD patterns of powders after heat treatment of n-butylamine (135°C) , 1-3 diaminopropane (255°C), DMC (300°C) and MIBK (220°C) syntheses.

The annealing temperatures were first determined by TGA. Indeed, upon annealing, the major mass loss corresponds to the elimination of the solvent molecules within the crystalline structure of the solvato-complex. Therefore, annealing temperatures were chosen in agreement with the principal mass loss relevant to the solvent removal (S4). The powders recovered after synthesis in butylamine, diaminopropane, DMC and MIBK were annealed at 135°C, 255°C, 300°C and 220°C respectively for 4 h. XRD patterns after annealing (Figure 2) show amorphous structures in the case of n-butylamine, DMC and MIBK while β -Li₃PS₄ was obtained in the case of diaminopropane. Strong fluorescence occurred with these annealed samples in Raman spectroscopy analysis at 532 nm. Additional Raman analysis was performed with a 1064 nm laser, which shows the presence of PS₄³⁻ units (421 cm⁻¹) and a peak characteristic of β -Li₃PS₄ at 173 cm⁻¹ for diaminopropane. An amorphous structure (two wide peaks between 150 and 300

cm⁻¹) was observed for n-butylamine (S2). It is worth noticing that the characteristic peaks of Li₂S are still visible on the diffractograms of the powders synthesized in amines and DMC due to incomplete reaction.

Electrochemical impedance measurements were performed after annealing or after synthesis for the solids prepared in solvents leading directly to Li₃PS₄ formation (PSH, THT, DMDS, PC and IBIB). All Nyquist plots are presented in supporting info S5. The ionic conductivities at 25°C are reported in table 2. Solids obtained in DMDS, DMC and PC exhibit negligible ionic conductivities. Compared to the other samples, IBIB combined with a low decomposition temperature leads to the material giving the highest ionic conductivity (2.1×10^{-4} S.cm⁻¹ at 25°C), which is higher than the values with THF (1.1×10^{-4} S.cm⁻¹) and with ACN (5.5×10^{-5} S.cm⁻¹) as solvents and reproduced from the literature in our labs. To the best of our knowledge, this ionic conductivity is the third highest for β-Li₃PS₄ obtained by wet chemical synthesis after the reported works of Yamamoto et al. ($\sigma_{25^\circ\text{C}} = 5.1 \times 10^{-4}$ S.cm⁻¹) and Marchini et al. ($\sigma_{25^\circ\text{C}} = 2.2 \times 10^{-4}$ S.cm⁻¹). To support the fact that the ionic conductivities are mainly driven by the choice of the solvent and the reactivity of the Li₂S-P₂S₅ system, packing density of several pellets was measured (table S1). The packing densities of materials synthesized in n-butylamine, PSH, THF and IBIB heat treated at 100 °C are respectively 64, 63, 64 and 61 %. Despite similar packing densities (less than 5% variation), we observe a very large difference of ionic conductivity (factor 10). It is worth mentioning that while the presence of Li₂S in the pellet is detrimental to the measured ionic conductivity, it does not significantly change the packing density of the pellets since the density of Li₃PS₄ and Li₂S are very close (1,78 and 1,66 respectively).

Solvents	Drying process (under vacuum)	Results after drying	Heat treatment	Ionic conductivity (S.cm ⁻¹)
n-butylamine	5H at 50°C	solvato-complex + Li ₂ S	4H at 135°C (Ar)	1.55 × 10 ⁻⁵
1-3 diaminopropane	5H at 140°C	solvato-complex + Li ₂ S	4H at 255°C (Ar)	7.58 × 10 ⁻⁶
PSH	4H at 25°C	amorphous + Li ₂ S	untreated	2.00 × 10 ⁻⁵
THT	4H at 25°C	amorphous + Li ₂ S	untreated	7.93 × 10 ⁻⁶
Thiophene	4H at 25°C	no reaction	untreated	not measured
DMDS	4H at 50°C	unknown phase + β Li ₃ PS ₄ + Li ₂ S	untreated	non-conductive
Sulfolane	3H at 260°C	no reaction	untreated	not measured
PC	13H at 120°C	amorphous	untreated	non-conductive
DMC	4H at 25°C	solvato-complex + β Li ₃ PS ₄ + Li ₂ S	4H at 300°C (Ar)	non-conductive
IBIB	4H at 120°C	β Li ₃ PS ₄	untreated	3.82 × 10 ⁻⁵
IBIB	4H at 25°C	Solvato-complex	2H at 100°C (Ar)	2,1 × 10 ⁻⁴
MIBK	5H at 120°C	solvato-complex and/or amorphous	4H at 220°C (Ar)	2.18 × 10 ⁻⁵
THF	4H at 25°C	Solvato-complex	4H at 100°C (Ar)	1,1 × 10 ⁻⁴
ACN	4H at 25°C	Solvato-complex	4H at 200°C (Ar)	5,5 × 10 ⁻⁵

Table 2 : Summary of syntheses and ionic conductivity at room temperature of powders

The ionic conductivity data for the materials obtained in the different solvents are compared in Figure 3 along with some reaction solvent parameters: boiling point, dielectric constant, Hansen parameter and electric dipole moment. Compounds with low conductivity (DMC, DMDS and PC) are not shown, and some data from the literature were added to complete the comparison : EA Yamamoto *et al.* (8) and EDA Ito *et al.* (25), DME Calpa *et al.* (18), anisole Maniwa *et al.* (36), N-methylformamide (NMF) Teragawa *et al.* (39) and methyl propyl ketone (MPK) Matsuda *et al.* (23). Identifying correlations between the solvent parameters and the ionic conductivity is difficult because of the Li₂S impurity, but it seems that a low dielectric constant and electric dipole moment as well as a medium Hansen's polarity parameter tend to promote the

reaction. The boiling point doesn't have a direct relationship with ionic conductivity but has an impact on the energy consumption to obtain a dried powder.

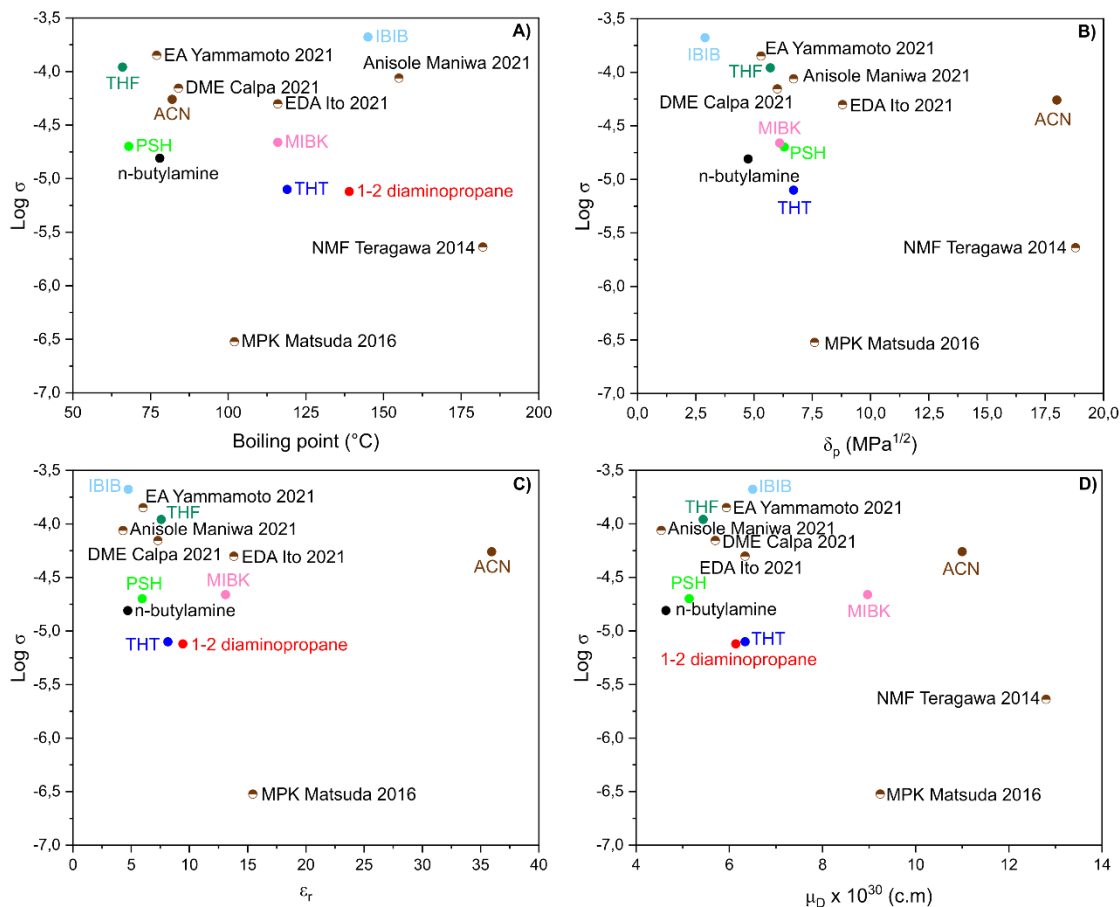


Figure 3 : Plot of ionic conductivity against boiling point (A), Hansen's polarity parameter (B), dielectric constant (C) and dipole moment (D) of different solvents

Regarding the reactivity in the tested solvents, only IBIB and MIBK with carbonyl functions allow the formation of $\text{Li}_3\text{PS}_4 \cdot x\text{Solvent}$ without traces of Li_2S . As described above, IBIB leads to a solvato-complex which decomposes into amorphous Li_3PS_4 below the boiling point, similar to the findings of Yamamoto *et al.* in butyl acetate (8). Indeed, they reported the solvato-complex $\text{Li}_3\text{PS}_4 \cdot 2\text{BA}$ has the ability to decompose at a temperature (100°C) lower than the solvent's

boiling point (126°C) to poorly crystallized Li_3PS_4 . The explanation of the low stability of the solvato-complex is based on the poor affinity of BA with PS_4^{3-} units, due to its low polarity represented by the Hansen polarity parameter δ_p in addition to low solvent molecule coordination number with Li_3PS_4 motifs. Accordingly, we believe that the unique behavior of IBIB is due to two factors. First, the Hansen polarity parameter δ_p of IBIB is 2,9, which is lower than that of BA (3,7), thus indicating a lower affinity. Second, the steric hindrance of IBIB, which is bulkier than BA and might further weaken the solvato-complex structure. The ionic conductivity of the Li_3PS_4 obtained in IBIB is lower than in BA ($2.1 \times 10^{-4} \text{ S.cm}^{-1}$ and $5 \times 10^{-4} \text{ S.cm}^{-1}$ respectively) but the synthesis method is also different. Indeed, in their study Yamamoto *et al.* used a “liquid shaking” synthesis technique with zirconia balls while in our case the synthesis was carried out by standard magnetic agitation. The higher conductivity of the amorphous Li_3PS_4 ($2.1 \times 10^{-4} \text{ S.cm}^{-1}$) compared to $\beta\text{-Li}_3\text{PS}_4$ ($3.82 \times 10^{-5} \text{ S.cm}^{-1}$) obtained in IBIB is in good agreement with previous works (8, 20, 27).

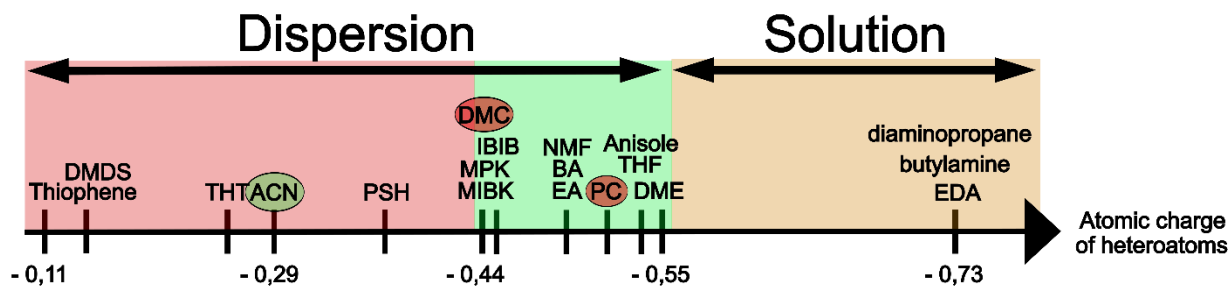


Figure 4 : Electronic charge of heteroatoms of solvent syntheses

From the results obtained in this study and those reported in the literature, the choice of the solvent has a critical impact on the $\text{Li}_2\text{S-P}_2\text{S}_5$ system’s reactivity. This can be explained by the interaction of the polar function of the solvent with the reactants which is driven by the electronic density. Hence, the partial charge of the solvent’s functional group is a key parameter for the reaction between Li_2S and P_2S_5 . This can be analyzed from the Mulliken charge of the

heteroatoms' polar function (Figure 4 and Table S2). According to our results, chemical groups with a nucleophilic function whose partial charge is in the range between -0.44 and -0.55 seem to be good candidates for Li_3PS_4 wet chemical synthesis. Below -0.44 the partial charge is not high enough to perform a complete reaction, except for the ACN case. On the other hand, a very high partial charge (-0.73) leads to the full dissolution of the precursors, but the interaction with the product, and thus its complexation, is too strong for a successful synthesis. Therefore, there is a trade-off between the interaction of the solvent with the reactant and products that can be quantified thanks to this descriptor.

The impact of the solvent's electronic density was previously studied with carbonyl based solvents by Matsuda *et al.* (23). They showed that acetates are better synthesis solvents than ketones, due to the stabilization of the PS_4^{3-} tetrahedra by the higher negative charge of the acetate function. Solids obtained in carbonates does not follow the trend due to residual impurities which may explain the lower ionic conductivity. In our case, the results with IBIB (ester) and MIBK (ketone) are in good agreement with Matsuda *et al.*, while the carbonates tend to react with Li_3PS_4 , releasing CO_2 . The comparison between THT and THF revealed that the reaction kinetics is slower in the case of THT compared to THF. Indeed, the reaction is not completed after 72 h at 50°C with THT while it is complete after 24 h at room temperature in THF. This could be due to the difference of electronegativity between sulfur and oxygen (2.58 vs. 3.44). The Mulliken charge of sulfur is indeed lower than that of oxygen and induces a lower stabilization of PS_4^{3-} compared to other chemical groups such as ester (EA) or ether (THF). This difference in stability impacts the reaction of $\text{Li}_2\text{P}_2\text{S}_6$ ·solvent at the surface of Li_2S and slows the kinetics down (eq 2). This is consistent with the systematic presence of residual Li_2S after

reaction in thiol and thioether. It is also highlighted by the fact that despite its protic nature, PSH doesn't solubilize Li_2S and P_2S_5 nor the solvato-complex, whereas amines do.

Furthermore, the presence of aromaticity on the thiophene ring doesn't enable the formation of the $\text{Li}_2\text{P}_2\text{S}_6 \cdot x\text{Solvent}$ intermediate and therefore the synthesis of the phase does not occur. This can be explained by a delocalization of the electron density over the whole molecule rather than a specific zone such as carbonyl. It thus prevents the complexation of the phase and does not allow the reaction between Li_2S and P_2S_5 to proceed. These results will be further reported in a forthcoming publication.

In their study, Gamo *et al.* (21) suggest that steric hindrance is a limiting factor in the synthesis of $\text{Li}_7\text{P}_3\text{S}_{11}$. In the case of the synthesis of Li_3PS_4 , it may not be the most limiting criterion at least in the considered range of solvent presented here. Indeed, the successful synthesis in IBIB shows that esters bulkier than acetates and propionates can be used for the wet chemical synthesis of Li_3PS_4 . The same assessment can be made with amines (1,3-diaminopropane compared with EDA), ketones (MIBK compared with methyl propyl ketone (MPK) (23)) as well as ethers (anisole compared with THF). It appears that bulkier solvents lead to a decrease in ionic conductivity, except for MIBK leading to a higher ionic conductivity than MPK, respectively $2.18 \times 10^{-5} \text{ S.cm}^{-1}$ and $3 \times 10^{-7} \text{ S.cm}^{-1}$ (23).

An optimum for LPS synthesis doesn't exist if one compares all chemical groups. An analysis of several factors with computer modeling may be helpful. But experimental data such as the unknown quantity of Li_2S after synthesis impacts the conductivity and could distort the results. Nevertheless, parameters such as boiling point, Hansen's polarity, dielectric constant and electric dipole moment can be used only to compare solvents in the same chemical family.

Another aspect not discussed yet is the synthesis method which can significantly impact the reaction kinetics and the resulting ionic conductivity. This discrepancy is widely described in the literature (1, 15, 28). Despite the solvent selection, wet chemical synthesis of Li_3PS_4 in the literature were conducted using standard agitation mode (9, 18, 25) (this work), liquid shaking with zirconia balls (8, 7), microwave heating (36, 40) and solvothermal conditions (41). Therefore, an accurate assessment of the effect of the solvent parameter extracted from the example of the literature would require a benchmark with the same synthesis method.

Conclusions

In this study we investigated eleven new polar solvents for the wet chemical synthesis of Li_3PS_4 . Six solvents (IBIB, n-butylamine, 1,3-diaminopropane, PSH, THT, MIBK) allow the formation of Li_3PS_4 with a measurable ionic conductivity. From these results, we compared the solvents on the basis of their ability to perform the reaction and the resulting ionic conductivity. The electronic density of the polar function of the solvent and more particularly the nucleophilic function brought by partial negative charge of the heteroatoms is critical for the formation of Li_3PS_4 . While carbonyl function in esters and ketones (-0.44 to -0.52) are sufficient to stabilize the PS_4^{3-} units, the lower charge of sulfur compared to oxygen slows the reaction kinetics. Moreover, the delocalization of the electronic density due to the presence of aromaticity severely disturbs the stability of the solvato-complex and prevents the reaction between Li_2S and P_2S_5 . Among the investigated solvents, IBIB exhibits a similar behavior to that of BA with a solvato-complex decomposition below the solvent's boiling point. The compound obtained after heat treatment at 100°C presents one of the highest ionic conductivities ($2.1 \times 10^{-4} \text{ S}\cdot\text{cm}^{-1}$) for this kind of synthesis method.

Supporting information

XRD pattern of Kapton + vacuum grease; Raman spectra of compounds subjected to fluorescence with 1064 nm laser; Characterizations (Raman spectra, XRD patterns, TGA and Nyquist plot) of $\text{Li}_3\text{PS}_4 \cdot \text{IBIB}$ dried at room temperature before and after heat treatment; TGA of solvato-complexes; Nyquist plots of all the Li_3PS_4 obtained after heat treatment; Calculated atomic charge of heteroatom of solvents.

Corresponding Author

*Cyril GARNERO cyril.garnero@ifpen.fr, IFP Energies Nouvelles, Etablissement de Lyon, BP3, 69360 Solaize, France

References

1. Ghidui, M.; Ruhl, J.; Culver, S. P.; Zeier, W. G. Solution-based synthesis of lithium thiophosphate superionic conductors for solid-state batteries: a chemistry perspective. *J. Mater. Chem. A* **2019**, *7* (30), 17735–17753. DOI: 10.1039/C9TA04772G.
2. Fan, L.; Wei, S.; Li, S.; Li, Q.; Lu, Y. Recent Progress of the Solid-State Electrolytes for High-Energy Metal-Based Batteries. *Adv. Energy Mater.* **2018**, *8* (11), 1702657. DOI: 10.1002/aenm.201702657.
3. Gobet, M.; Greenbaum, S.; Sahu, G.; Liang, C. Structural Evolution and Li Dynamics in Nanophase Li_3PS_4 by Solid-State and Pulsed-Field Gradient NMR. *Chem. Mater.* **2014**, *26* (11), 3558–3564. DOI: 10.1021/cm5012058.
4. TACHEZ, M.; MALUGANI, J.; MERCIER, R.; ROBERT, G. Ionic conductivity of and phase transition in lithium thiophosphate Li_3PS_4 . *Solid State Ionics* **1984**, *14* (3), 181–185. DOI: 10.1016/0167-2738(84)90097-3.
5. Deiseroth, H.-J.; Kong, S.-T.; Eckert, H.; Vannahme, J.; Reiner, C.; Zaiß, T.; Schlosser, M. $\text{Li}_6\text{PS}_5\text{X}$: A Class of Crystalline Li-Rich Solids With an Unusually High Li^+ Mobility. *Angew. Chem.* **2008**, *120* (4), 767–770. DOI: 10.1002/ange.200703900.
6. Liang, F.; Sun, Y.; Yuan, Y.; Huang, J.; Hou, M.; Lu, J. Designing inorganic electrolytes for solid-state Li-ion batteries: A perspective of LGPS and garnet. *Materials Today* **2021**, *50*, 418–441. DOI: 10.1016/j.mattod.2021.03.013.
7. Yamamoto, K.; Takahashi, M.; Ohara, K.; Phuc, N. H. H.; Yang, S.; Watanabe, T.; Uchiyama, T.; Sakuda, A.; Hayashi, A.; Tatsumisago, M. *et al.* Synthesis of Sulfide Solid Electrolytes through the

- Liquid Phase: Optimization of the Preparation Conditions. *ACS omega* **2020**, *5* (40), 26287–26294. DOI: 10.1021/acsomega.0c04307.
8. Yamamoto, K.; Yang, S.; Takahashi, M.; Ohara, K.; Uchiyama, T.; Watanabe, T.; Sakuda, A.; Hayashi, A.; Tatsumisago, M.; Muto, H. *et al.* High Ionic Conductivity of Liquid-Phase-Synthesized Li₃PS₄ Solid Electrolyte, Comparable to That Obtained via Ball Milling. *ACS Appl. Energy Mater.* **2021**, *4* (3), 2275–2281. DOI: 10.1021/acsaem.0c02771.
 9. Liu, Z.; Fu, W.; Payzant, E. A.; Yu, X.; Wu, Z.; Dudney, N. J.; Kiggans, J.; Hong, K.; Rondinone, A. J.; Liang, C. Anomalous high ionic conductivity of nanoporous β -Li₃PS₄. *Journal of the American Chemical Society* **2013**, *135* (3), 975–978. DOI: 10.1021/ja3110895.
 10. Ghidui, M.; Schlem, R.; Zeier, W. G. Pyridine Complexes as Tailored Precursors for Rapid Synthesis of Thiophosphate Superionic Conductors. *Batteries & Supercaps* **2021**, *4* (4), 607–611. DOI: 10.1002/batt.202000317.
 11. Duchardt, M.; Diels, M.; Roling, B.; Dehnen, S. Flow-Oriented Synthesis of Li₂S and Li₃PS₄·3THF: Opening Up a Completely Solvent-Based Solid Electrolyte Value Chain. *ACS Appl. Energy Mater.* **2020**, *3* (7), 6937–6945. DOI: 10.1021/acsaem.0c01007.
 12. Subramanian, Y.; Rajagopal, R.; Ryu, K.-S. High ionic-conducting Li-argyrodites synthesized using a simple and economic liquid-phase approach and their application in all solid-state-lithium batteries. *Scripta Materialia* **2021**, *204*, 114129. DOI: 10.1016/j.scriptamat.2021.114129.
 13. Yubuchi, S.; Uematsu, M.; Hotehama, C.; Sakuda, A.; Hayashi, A.; Tatsumisago, M. An argyrodite sulfide-based superionic conductor synthesized by a liquid-phase technique with tetrahydrofuran and ethanol. *J. Mater. Chem. A* **2019**, *7* (2), 558–566. DOI: 10.1039/C8TA09477B.
 14. Zhou, L.; Park, K.-H.; Sun, X.; Lalère, F.; Adermann, T.; Hartmann, P.; Nazar, L. F. Solvent-Engineered Design of Argyrodite Li₆PS₅X (X = Cl, Br, I) Solid Electrolytes with High Ionic Conductivity. *ACS Energy Lett.* **2019**, *4* (1), 265–270. DOI: 10.1021/acseenergylett.8b01997.
 15. Banik, A.; Famprakis, T.; Ghidui, M.; Ohno, S.; Kraft, M. A.; Zeier, W. G. On the underestimated influence of synthetic conditions in solid ionic conductors. *Chemical science* **2021**, *12* (18), 6238–6263. DOI: 10.1039/d0sc06553f.
 16. Lee, J. E.; Park, K.-H.; Kim, J. C.; Wi, T.-U.; Ha, A. R.; Song, Y. B.; Oh, D. Y.; Woo, J.; Kweon, S. H.; Yeom, S. J. *et al.* Universal Solution Synthesis of Sulfide Solid Electrolytes Using Alkahest for All-Solid-State Batteries. *Advanced materials (Deerfield Beach, Fla.)* **2022**, *34* (16), e2200083. DOI: 10.1002/adma.202200083.
 17. Calpa, M.; Rosero-Navarro, N. C.; Miura, A.; Terai, K.; Utsuno, F.; Tadanaga, K. Formation Mechanism of Thiophosphate Anions in the Liquid-Phase Synthesis of Sulfide Solid Electrolytes Using Polar Aprotic Solvents. *Chem. Mater.* **2020**, *32* (22), 9627–9632. DOI: 10.1021/acs.chemmater.0c03198.
 18. Calpa, M.; Nakajima, H.; Mori, S.; Goto, Y.; Mizuguchi, Y.; Moriyoshi, C.; Kuroiwa, Y.; Rosero-Navarro, N. C.; Miura, A.; Tadanaga, K. Formation Mechanism of β -Li₃PS₄ through Decomposition of Complexes. *Inorganic chemistry* **2021**, *60* (10), 6964–6970. DOI: 10.1021/acs.inorgchem.1c00294.

19. Delnick, F. M.; Yang, G.; Self, E. C.; Meyer, H. M.; Nanda, J. Investigation of Complex Intermediates in Solvent-Mediated Synthesis of Thiophosphate Solid-State Electrolytes. *J. Phys. Chem. C* **2020**, *124* (50), 27396–27402. DOI: 10.1021/acs.jpcc.0c08761.
20. Marchini, F.; Porcheron, B.; Rousse, G.; Albero Blanquer, L.; Droguet, L.; Foix, D.; Koç, T.; Deschamps, M.; Tarascon, J. M. The Hidden Side of Nanoporous β -Li₃PS₄ Solid Electrolyte. *Adv. Energy Mater.* **2021**, *11* (34), 2101111. DOI: 10.1002/aenm.202101111.
21. Gamo, H.; Nagai, A.; Matsuda, A. The effect of solvent on reactivity of the Li₂S-P₂S₅ system in liquid-phase synthesis of Li₇P₃S₁₁ solid electrolyte. *Scientific reports* **2021**, *11* (1), 21097. DOI: 10.1038/s41598-021-00662-3.
22. Wang, Y.; Lu, D.; Bowden, M.; El Khoury, P. Z.; Han, K. S.; Deng, Z. D.; Xiao, J.; Zhang, J.-G.; Liu, J. Mechanism of Formation of Li₇P₃S₁₁ Solid Electrolytes through Liquid Phase Synthesis. *Chem. Mater.* **2018**, *30* (3), 990–997. DOI: 10.1021/acs.chemmater.7b04842.
23. Matsuda, A.; Muto, H.; H.H. PHUC, N. Preparation of Li₃PS₄ Solid Electrolyte by Liquid-Phase Shaking Using Organic Solvents with Carbonyl Group as Complex Forming Medium. *J. Jpn. Soc. Powder Powder Metallurgy* **2016**, *63* (11), 976–980. DOI: 10.2497/jjspm.63.976.
24. Zhou, J.; Chen, Y.; Yu, Z.; Bowden, M.; R. S. Miller, Q.; Chen, P.; Schaefer, H. T.; Mueller, K. T.; Lu, D.; Xiao, J. *et al.* Wet-chemical synthesis of Li₇P₃S₁₁ with tailored particle size for solid state electrolytes. *Chemical Engineering Journal* **2022**, *429*, 132334. DOI: 10.1016/j.cej.2021.132334.
25. Ito, A.; Kimura, T.; Sakuda, A.; Tatsumisago, M.; Hayashi, A. Liquid-phase synthesis of Li₃PS₄ solid electrolyte using ethylenediamine. *J Sol-Gel Sci Technol* **2021**, *101*, 2-7. DOI: 10.1007/s10971-021-05524-y.
26. Kimura, T.; Ito, A.; Nakano, T.; Hotehama, C.; Kowada, H.; Sakuda, A.; Tatsumisago, M.; Hayashi, A. Crystalline precursor derived from Li₃PS₄ and ethylenediamine for ionic conductors. *J Sol-Gel Sci Technol* **2022**, *104*, 1-8 DOI: 10.1007/s10971-022-05824-x.
27. Takahashi, M.; Yang, S.; Yamamoto, K.; Ohara, K.; Phuc, N. H. H.; Watanabe, T.; Uchiyama, T.; Sakuda, A.; Hayashi, A.; Tatsumisago, M. *et al.* Improvement of lithium ionic conductivity of Li₃PS₄ through suppression of crystallization using low-boiling-point solvent in liquid-phase synthesis. *Solid State Ionics* **2021**, *361*, 115568. DOI: 10.1016/j.ssi.2021.115568.
28. Gamo, H.; Nagai, A.; Matsuda, A. Toward Scalable Liquid-Phase Synthesis of Sulfide Solid Electrolytes for All-Solid-State Batteries. *Batteries* **2023**, *9* (7), 355. DOI: 10.3390/batteries9070355.
29. Delley, B. Fast Calculation of Electrostatics in Crystals and Large Molecules. *J. Phys. Chem.* **1996**, *100* (15), 6107–6110. DOI: 10.1021/jp952713n.
30. Baker, J.; Kessi, A.; Delley, B. The generation and use of delocalized internal coordinates in geometry optimization. *J. Chem. Phys.* **1996**, *105* (1), 192–212. DOI: 10.1063/1.471864.
31. Becke, A. D. Density-functional thermochemistry. III. The role of exact exchange. *J. Chem. Phys.* **1993**, *98* (7), 5648–5652. DOI: 10.1063/1.464913.
32. Stephens, P. J.; Devlin, F. J.; Chabalowski, C. F.; Frisch, M. J. Ab Initio Calculation of Vibrational Absorption and Circular Dichroism Spectra Using Density Functional Force Fields. *J. Phys. Chem.* **1994**, *98* (45), 11623–11627. DOI: 10.1021/j100096a001.

33. Ohsaki, S.; Yano, T.; Hatada, A.; Nakamura, H.; Watano, S. Size control of sulfide-based solid electrolyte particles through liquid-phase synthesis. *Powder Technology* **2021**, *387*, 415–420. DOI: 10.1016/j.powtec.2021.04.050.
34. Wissel, K.; Riegger, L. M.; Schneider, C.; Waidha, A. I.; Famprakis, T.; Ikeda, Y.; Grabowski, B.; Dinnebier, R. E.; Lotsch, B. V.; Janek, J. *et al.* Dissolution and Recrystallization Behavior of Li₃PS₄ in Different Organic Solvents with a Focus on N-Methylformamide. *ACS Appl. Energy Mater.* **2023**, *6* (15), 7790–7802. DOI: 10.1021/acsaem.2c03278.
35. Phuc, N. H. H.; Morikawa, K.; Totani, M.; Muto, H.; Matsuda, A. Chemical synthesis of Li₃PS₄ precursor suspension by liquid-phase shaking. *Solid State Ionics* **2016**, *285*, 2–5. DOI: 10.1016/j.ssi.2015.11.019.
36. Maniwa, R.; Calpa, M.; Rosero-Navarro, N. C.; Miura, A.; Tadanaga, K. Synthesis of sulfide solid electrolytes from Li₂S and P₂S₅ in anisole. *J. Mater. Chem. A* **2021**, *9* (1), 400–405. DOI: 10.1039/D0TA08658D.
37. M. Somer, W. Bues and W. Brückner. Schwingungsspektren von Tetraphosphordekasulfid P₄S₁₀. *Z. Naturforsch.* **1983**, *38.a*, 163–166.
38. SHIMAMOTO, K.; Sakuda, A.; Hayashi, A.; Tatsumisago, M. Characterization of quasi-solid electrolytes based on Li₃PS₄ glass with organic carbonate additives. *J. Ceram. Soc. Japan* **2020**, *128* (9), 653–655. DOI: 10.2109/jcersj2.20114.
39. Teragawa, S.; Aso, K.; Tadanaga, K.; Hayashi, A.; Tatsumisago, M. Liquid-phase synthesis of a Li₃PS₄ solid electrolyte using N-methylformamide for all-solid-state lithium batteries. *J. Mater. Chem. A* **2014**, *2* (14), 5095. DOI: 10.1039/c3ta15090a.
40. Suto, K.; Bonnicksen, P.; Nagai, E.; Niitani, K.; Arthur, T. S.; Muldoon, J. Microwave-aided synthesis of lithium thiophosphate solid electrolyte. *J. Mater. Chem. A* **2018**, *6* (43), 21261–21265. DOI: 10.1039/C8TA08070D.
41. Choi, S.; Lee, S.; Park, J.; Nichols, W. T.; Shin, D. Facile synthesis of Li₂S-P₂S₅ glass-ceramics electrolyte with micron range particles for all-solid-state batteries via a low-temperature solution technique (LTST). *Applied Surface Science* **2018**, *444*, 10–14. DOI: 10.1016/j.apsusc.2018.02.270.